ROOTINDEXING
JOURNAL ABSTRACTING AND INDEXING SERVICE
INTERNATIONAL ADVANCE JOURNAL OF ENGINEERING, SCIENCE AND MANAGEMENT (IAJESM)
July-December 2023, Submitted in July 2023, iajesm2014@gmail.com, ISSN -2393-8048
Multidisciplinary Indexed/Peer Reviewed Journal. SJIF Impact Factor 2023 =6.753

BLOCK COPOLYMER MEDIATED SYNTHESIS OF Pdqds: REDUCTION OF Cr (VI)TO Cr (III)

Seema Singh, Researcher (Chemistry Department), Sardar Patel University, Balaghat (Madhya Pradesh)
Dr. Praveen Kumar, Associate Professor (Chemistry Department), Sardar Patel University, Balaghat (Madhya Pradesh)

ABSTRACT

This study presents a revolutionary one-pot Palladium Quantum Dot (PdQD) production process with disruptive potential and broad applicability. The method's simplicity, room-temperature operation, and lack of harsh chemicals make it easy to implement without specific equipment. A sigmoidal curve in absorption-based time scan spectra shows monodispersed PdQDs with autocatalytic development, validating the synthesis. Due to their tiny size and homogeneity, PdQDs are excellent catalysts for the room-temperature reduction of hazardous Cr(VI) to Cr(III) in acetic acid. Catalytic behaviour is due to quantum dots' large surface areas. The catalyst can be recycled through γ irradiation-induced aggregation and precipitation, although with reduced efficiency due to bigger nanoparticles. PdQDs show potential as catalysts in Cr(VI) reduction systems, as evidenced by their significant and quantifiable reactivity to γ i Combining Pd with γ irradiation has potential for catalytic processes in research and practical applications, despite its high cost.

Keywords: Palladium Quantum Dot, Cr(VI) to Cr(III), Catalytic Processes

INTRODUCTION

Compared to their bulk equivalents, quantum dots (QDs) exhibit unique electrical, magnetic, optical, chemical, and mechanical properties that depend on their size (Jiang et al., 2007). These tiny magic dots have countless potential uses, all of which necessitate a straightforward process using safe chemicals. Uddandarao and Mohan (2016) and Tu et al. (2016) are two sources that state that there are currently efforts to synthesise semiconductor quantum dots in a more environmentally friendly way. The greener synthesis of PdQDs, however, has received very less attention. The stated methods also have a number of drawbacks, such as the fact that their syntheses necessitate extreme conditions like high pressure, heat, or an inert atmosphere, among other complicated requirements. Synthesis employing simple biocompatible and biodegradable reactants involves experimental settings that are difficult to sustain, and there are just a few mentions of this in the literature. Table 1 shows that PdQDs and other noble metal NPs have been synthesised under harsh and challenging conditions using other methods from the one utilised in this study.

Table 1: Several reported methods for the synthesis of PdQDs(<5nm) /NPs

Size (nm)	Chemicals	Conditions	Application	Ref
1-3	Palladium complexes of type [Pd(L)Cl]Cl=(1–3) (where pincer ligand L = L1–L3 = $(ArECH_2CH_2)_2NH$; (E = S/Se/Te))4-bromobenzoic acid, phenylboronic acid, K_2CO_3, $CHCl_3$ CH_3–COO-CH_2– CH_3	heating at 100 °C for 5 h	Suzuki coupling reactions	Kumar et al.,2013
3.5	$Pd(OAc)_2$, ionic liquids $[But_3PC_{10}H_{21}][BF_4]$, $[But_3PC_{10}H_{21}][Tf2N]$, C_2H_5OH	stirring for 15 min at RT	interaction of imidazolium-based ILs with Pd NPs	Zvereva etal., 2014
4-7	Gelatin, $PdCl_2$	refluxing for 5 h	ligand- and amine-free Sonogashira–Hagihara reaction	Firouzabadi et al., 2011

3	Ionic liquids [EMI][MeHPO$_3$], [BMI][NTf$_2$] (BMI = 1-butyl-3- methyl-imidazolium) and [BMP][NTf$_2$] (BMP = N-butyl-N- methy pyrrolidinium), [Pd2(dba)$_3$], dipalladium tris (dibenzylideneacetone)	stirring at RT under argon. system was pressurized with hydrogen (3 bar) and stirred at 50- 80 ˚C overnight	C–C coupling/reduction tandem process	Raluy et al., 2011
2-4	K$_2$PdCl$_4$, 2 diaminobenzene, CH$_3$-OH	R.T., 2 h	Suzuki coupling reaction	Taher et al.,2015
3	p-amino-acetanilide, CH$_3$-OH, PdC$_4$H$_6$O$_4$		Suzuki cross-coupling reactions	Islam et al.,2011
5	MTO$_x$-3DG, PdCl$_2$, ascorbic acid	grinding for 5 min	direct ethylene glycol fuel cells and oxygen evolution reactions	Kannan et al.,2016
5	PdCl$_2$, PVP, NaI	heated at 180 ˚C for 1.5 h	Photoelectrocatalytic glucose oxidation	Zhang et al.,2015
5.3	PVA, Na$_3$C$_6$H$_5$O$_7$	refluxed continuously with an occasional flow of nitrogen gas into the reaction mixture for 2h and 20 min	electrocatalytic activity	Roy et al.,2010
2.2	C$_2$H$_5$OH, DIB/PEI/RGO, HCHO, hexane, CHCl$_3$	stirred for 2 h, N$_2$ atmosphere	catalytic reduction of 4-nitrophenol	Su et al.,2016
3.8	Reduced graphene oxide, PdCl$_2$	ultrasoncation and agitation for 1 h	----	Zhanga et al.,2016
1–3	K$_2$PdCl$_4$, TOAB was dissolved in toluene.,octadecanethiol or octadecylamine, NaBH$_4$	sonication, rotary evaporation, overnight stirring	additive for the hydrocarbon fuel	Yue et al.,2016

Table 6.1 (contd.)

1.4	Hydroxyl terminated sixth- generation(G6-OH) (PAMAM),(K$_2$PdCl$_4$)	stirring for 30 min, NaBH$_4$	oxidation of morin	Ncube et al., 2015
2	Pd(OAc)$_2$, Mesyl–PEG–OMe,CH$_2$Cl$_2$, n-hexane	stirred at room temperature for 3 h, dried by vacuum	nitrile hydration to amide in water	Oberhauser aet al., 2015
5	Insulin peptide, Na$_2$PdCl$_4$	incubated at 70 ◦C for three days, aged at 25C for two days	Suzuki coupling reactions	Zhoua et al., 2015

4.8	Gum ghatti, $PdCl_2$	autoclaving at 121˚C and 103 kPa for 30 min	catalytic degradation of coomassie brilliant blue and antibacterial activity	Kora, and Rastogi, 2015
variable	Silicon wafer, polystyrene, poly(methyl methacrylate), $CHCl_3$	Ar during sputtering and N_2 environment for annealing temperature range 95°C-240°C and time 3600–10,800 s	----	Ruffino et al., 2012
2-3	Pyromellitic dianhydride-4 ,48 oxydianilinepolyimide, puresilica matrix	ion energy of 100 kev, sample holder was water-cooled	-------	Maggioniet al., 2004
variable	Glass slides , acidic bath, poly(*N*- vinylcarbazole), toluene	N_2 for drying of sample, toluene and permanent stirring,spin-coating with 2000 rpm for 120 s	----	Kaune et al., 2009
12-60	SiC substrates n-type with a doping concentration ND≈5.1 X 1017 cm^{-3}, Si terminated, Pd source ≈99.999% purity target	Ar during sputtering ,15 to 360 s	----	Ruffino, and Grimaldi, 2010
2-3	$PdCl_2$, ethanolic solution of block copolymer (PEG-PPG-PEG)	R.T., 5 min	catalytic reduction of Cr(VI) to Cr(III)	This work

MTOx-3DG=manganese-titanium oxide/3D graphene; PVP= polyvinylpyrrolodine; PVA= polyvinylalcohol TOAB= tetraoctylammonium bromide; RGO= Reduced graphene oxide; PEI= polyetheylenimine; DIB= 3,4-dihydroxybenzaldehyde ; PAMAM= poly(amidoamine)

The two most common chromium oxidation states are Cr(III) and Cr(VI). Because of its reduced solubility, reactivity, and mobility in the environment, Cr(III) is less harmful to living beings than the other dominant oxidation state. Alternatively, Cr(VI) is notorious for its cancer-causing, mutagenesis, and acute toxic effects (Elliott and Zhang, 2001). Its increased water solubility, quick translocation through biological membranes, and subsequent interactions with nucleic acids and proteins within cells make it more hazardous than Cr(III). Additionally, it is acknowledged as a highly significant and pervasive environmental pollutant. One easily implementable strategy to address the problem of chromium pollution is the conversion of electron deficient Cr(VI) to electron rich Cr(III) (Omole et al., 2007).

CHEMICALS AND REAGENTS

A source of palladium chloride was LOBA chemicals. The composition of this substance is PEG-PPG-PEG, which stands for poly(ethylene glycol)-block-poly(propylene glycol). Sigma-Aldrich supplied the Mn=5800. Aqueous acid and potassium dichromate were procured from MERCK. A source of ethanol was SRL chemicals. Throughout the experiment, solutions were prepared using triple-distilled water.

INSTRUMENTS

(i) Methods based on microscopy, such as scanning transmission electron microscopy (STEM), electron diffraction (ED), atomic force microscopy (AFM), scanning electron energy loss spectroscopy (EELS), scanning electron microscopy (SEM), and high-resolution transmission electron microscopy (HRTEM).

(ii) Methods that rely on X-rays, such as X-ray diffractometry (XRD), X-ray photoelectron spectroscopy (XPS), X-ray absorption spectroscopy (XAS), short-angle X-ray scattering (SAXS), and extended X-ray absorption near edge structure (EXAFS).

(iii) Different methods for characterising the substance can be used, such as ultraviolet-visible (UV-Vis) spectroscopy, photoluminescence (PL) spectroscopy, dynamic light scattering (DLS), zeta potential (ν-potential), SQUID, vibrating sample magnetometry (VSM), infrared spectroscopy (IR), nuclear magnetic resonance (NMR), thermal gravimetric analysis (TGA), mass spectrometry (MS),, etc. The gamma irradiation was carried out in a 60Co radiation chamber at a dosage rate of 2.249 kGy/h.

SYNTHESIS OF QDs

A 2 mL solution of palladium chloride with a concentration of 1 mM was combined with 3 mL of a 1% PEG-PPG-PEG block copolymer produced in ethanol. The mixture was then let to stand at room temperature for 5 minutes in order to synthesise the PdQDs. Further characterization was carried out on the colourless solution that had turned brown, indicating the production of nanoparticles.

CMC MEASUREMENT

Micelles exist in solution at concentrations exceeding the critical molecular concentration (CMC) of surfactants or polymers in bulk. The conductance values of solutions containing ethanol and varying concentrations of the block copolymer, ranging from 0.2% to 1.2% by weight, were recorded. The CMC value of the block copolymer was determined by plotting conductance against concentration. Our study's CMC was calculated by squaring two straight lines drawn from conductance against surfactant concentration plots, which we collected from experimental data of a block copolymer solution with escalating concentrations (Samaddar et al., 2015). Conductance values of the block copolymer at various concentrations are shown in Figure 1. It is suggested that the CMC value of this polymer is around 0.6% (w/v) concentration by the junction of the two lines.

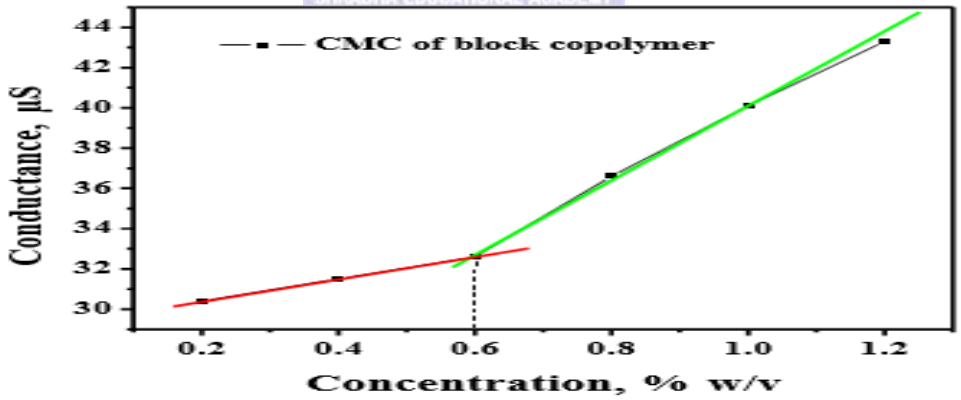

Figure 1: Conductance of different concentrations of block copolymer solutions for obtaining the CMC

STUDIES ON CHARACTERISATION

Measuring absorption spectra

Nanoparticle formation in the block copolymer medium was confirmed by the absorption spectroscopy. As the concentration of Pd(II) increased from 0.0196 to 0.0654 mM, the 1% block copolymer solution's absorbance at 300 nm (λ_{max}) changed. In order to track the QDs' development kinetics, we also monitored the absorbance change over time for each of the aforementioned sets.

Typical plasmonic resonances are seen in very few metallic nanoparticles, including palladium and platinum (Wojnicki et al., 2016). One visible sign of Pd(II) reduction to Pd(0) was the solution's colour changing from yellow to a dark brown colloid. Keeping an eye on the solution's absorption spectra verifies this. In this region (200-450 nm), the sharp peak at 430 nm for Pd(II) (figure 2a) disappeared, suggesting that the concentration of Pd(II) ions has been reduced. As the concentration of Pd(II) in the solution increased, there was a subsequent and continuous rise in the absorption band at a range of 200 nm to 450 nm. A large body of prior research (Roy et al., 2010; Yue et al., 2016) also lends credence to this distinguishing fact. Small spherical PdQDs with a size less than 10 nm display surface plasmon resonance (SPR) between the 200 nm to 300 nm range, as previously noted by Ncube et al. (2015). There is no change in the peak position (λmax) of the solution containing PdQDs with increasing concentration of the added Pd(II) ions, suggesting a uniform particle size distribution, as shown in Figure 2b, the absorption spectrum of the synthesised PdQDs (He et al., 2005).

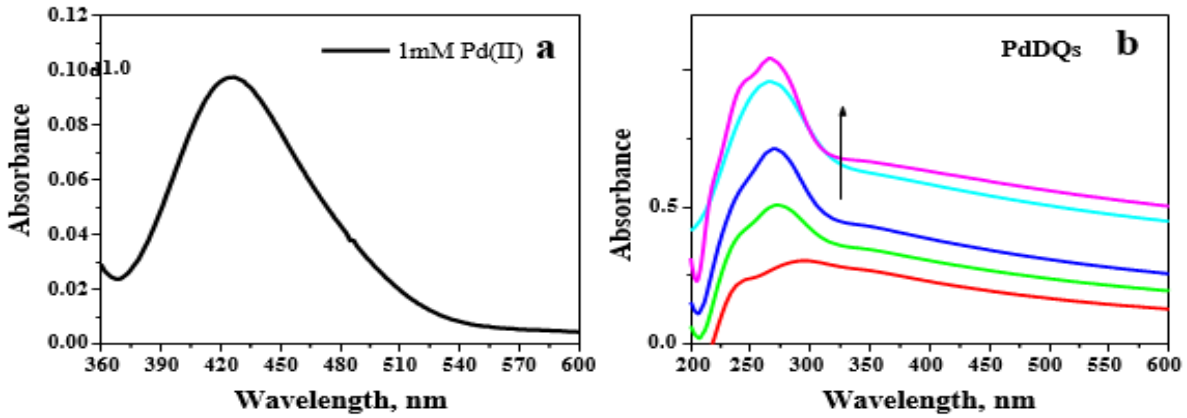

Figure 2a: Absorption spectrum of divalent Pd(II) ,2b: Absorption spectra of PdQD with increasing Pd(II)concentration

In order to determine the unknown concentration of PdQDs in solution, the slope of the calibration plot showing absorbance vs. concentration of PdQDs (figure 2c) was utilised, with the peak at λ_{max} 300 nm being taken into account. So, it was determined that the PdQD concentration in the solution set made according to the aforementioned method, which contained 0.16 mM of Pd(II), was 0.119 mM.

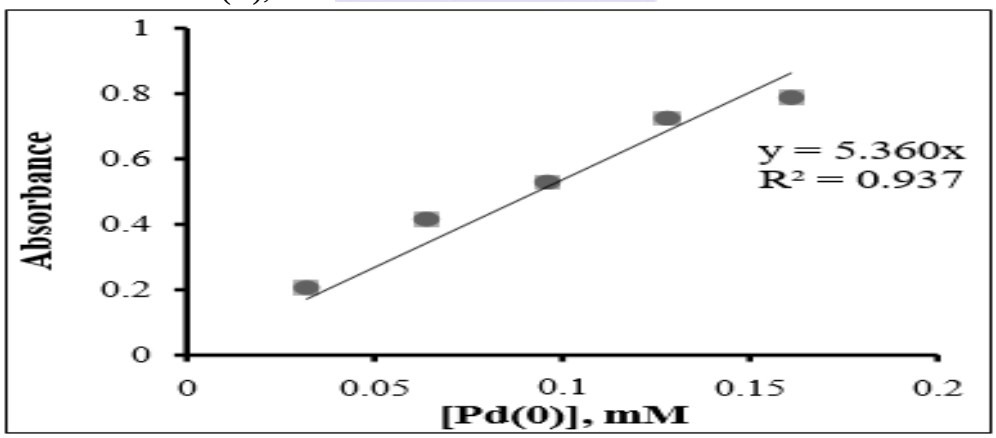

Figure 2c: Calibration curve of PdQDs

TEM analysis

Before taking TEM pictures, the PdQD solution was dropped onto a carbon-coated copper grid and allowed to dry under an infrared lamp. The TEM micrograph verified the size and shape of the produced PdQDs. Verified by Figure 3a, the creation of PdQDs smaller than 5 nm verifies that these particles possess quantum dot dimensions. Figure 3b, the TEM histogram, reveals a very limited range of deviation in the size distribution, indicating a homogeneous particle size distribution. The crystalline character of the QDs is confirmed by the SAED pattern (figure 3c). According to Chawla et al. (2016), the five bright concentric rings observed

in the image are caused by reflections from the (111), (200), (220), (311) and (222) planes, which are characteristic of the fcc lattice structure of the PdQDs. The EDX spectrum of the PdQDs, as shown in Figure 3d, further confirms that the synthesised QDs include palladium.

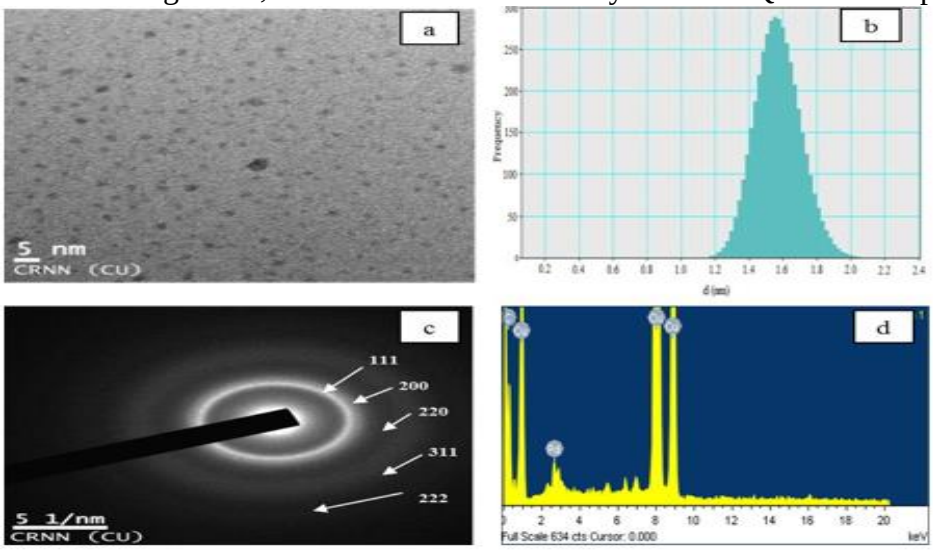

Figure 3a: TEM image (b) Histogram (c) SAED pattern and (d) EDX spectra of PdQD

DLS and ζ potential measurements

Additionally, the ready-made QD solutions had their DLS and ξ potentials assessed. Particles measuring around 200 nanometers in size are represented by the DLS profile. Because the PdQDs are encased in a polymeric coating of the block copolymer, the extremely high hydrodynamic radius of the colloidal solution containing these particles may be explained. Previous reports have also noted that the DLS experiment revealed a greater radius of the micellar arrangement generated by the block copolymer (Umapathi and Venkatesu, 2016). In Figure 4, we can see the DLS-obtained size distribution of the synthesised PdQDs. The values of the zeta potential show how much electrostatic repulsion there is in the colloidal solution between particles with the same charge.

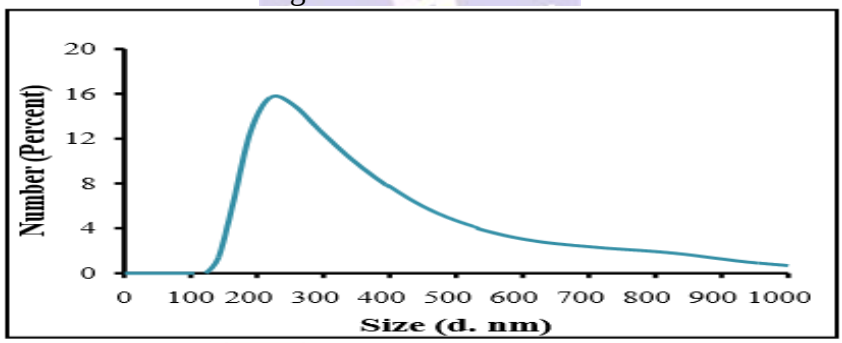

Figure 4: DLS data of PdQDs

The zeta potential values of the micellar dispersion of the solutions containing the block copolymer and the PdQDs are summarised in Table 2. In most cases, the terminal carboxylic acid groups encase particles in a negative charge, which helps to stabilise them. As a result of their electrostatic repulsion interactions, the negatively charged moiety aids in preventing agglomeration (Arora et al., 2016).

Table 2: Zeta potential of PdQDs

Sample	Zeta potential (mV)	Conductivity (ms/cm)
1% Block copolymer	-1.88±0.018	0.0104±0.0005
PdQDs	-3.71±0.037	0.7550±0.0375

IR analysis

We also used infrared spectra to look into how the block copolymer helped create and stabilise the PdQD. Several functional groups can be observed in the chemical structure of the block copolymer (scheme 1).

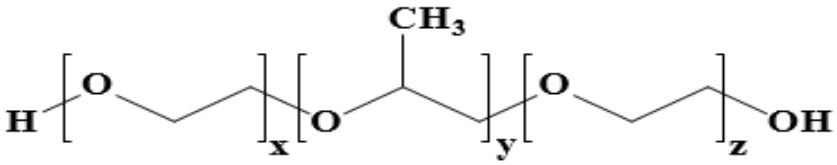

Scheme 1: Chemical structure of the block copolymer

The block copolymer's infrared spectra display a peak at 3436 cm^{-1}, which is attributed to the -OH stretching frequency (figure 5).

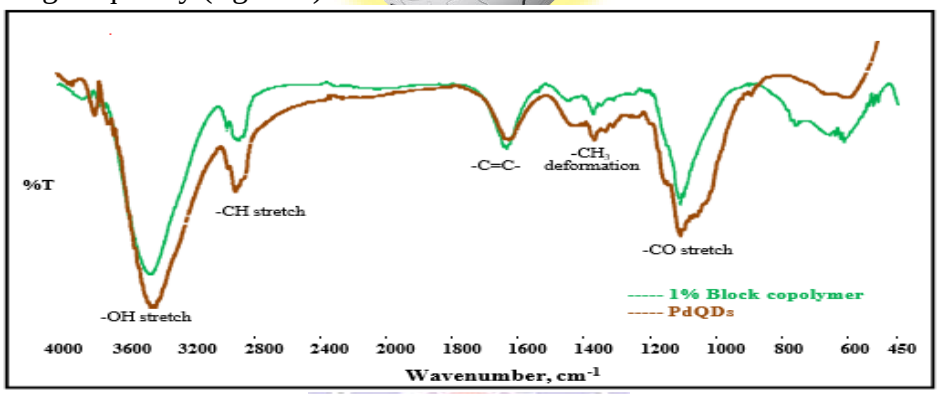

Figure 5: IR spectra of block copolymer and PdQDs

According to previous research on metal nanoparticles coated with polymers, specific functional groups have a crucial role in keeping them stable (Islam et al., 2011). This is primarily caused by the steric effect imposed by the polymeric chain and the coordination of the functional groups to the surface of the nanoparticle. We discovered that the -OH group is involved in stabilising the PdQDs in our experiment. There is weak coordinative bonding between the -OH group and PdQDs, since the peak at 3413 cm^{-1} was moved down from its initial location at 3436 cm^{-1} (Roy et al., 2010). Table 3 provides a summary of the infrared frequencies observed in the block copolymer and the PdQDs that were synthesised. The -CH, -CH3, -C=C-, and -CO functional groups are represented by the peaks at 2903 cm^{-1}, 1374 cm^{-1}, 1636 cm^{-1}, and 1109 cm^{-1}, respectively. The bands corresponding to -CO and C=C stretch are caused by the residual carbonyl group that is left over after the polymer is hydrolyzed and rearranged. Any shift in the relative positions of these vibrational frequencies points to the block copolymer moiety's role in PdQD generation and stabilisation.

Table 3: IR spectral data of block copolymer and PdQDs

Functional group	Vibrational frequency (cm^{-1})	
	1% Block copolymer	PdQDs
-OH stretch	3436	3413
-CH stretch	2903	2922
-C=C-	1636	1632
-CH3 deformation	1374	1373
-CO stretch	1109	1112

MECHANISM

In standard nanosynthesis, an appropriate reducing agent is used to lower the ion concentration of the precursor metal. Surface protection of the produced nanoparticles is necessary to avoid agglomeration and stabilise the nanoparticle colloidal solution. Stabilising agents are typically used to do this. However, the present study found that block copolymers are capable of effectively performing both the reduction and stabilisation functions. To stabilise nanoparticles, polymers often employ steric crowding and weak binding to the surface of the particles through heteroatoms, effectively serving as both a ligand and a stabiliser. Block copolymers are appealing because they preserve the surface activity of the enclosed nanostructure by not passivating its surface (Bortolotto et al., 2015).

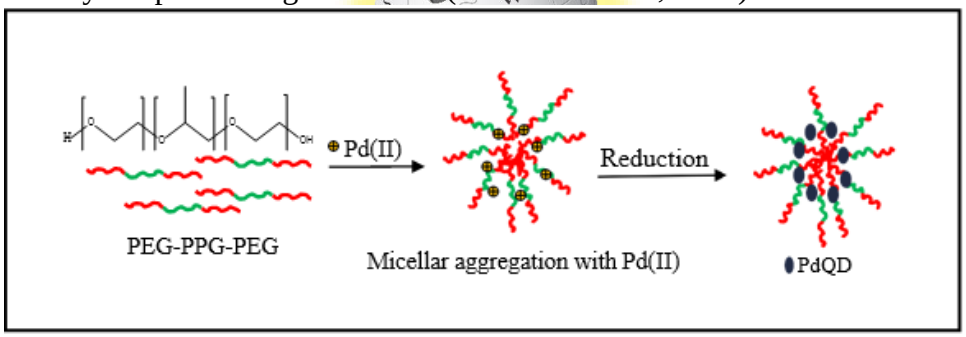

Figure 6: Schematic representation of the plausible mechanism of PdQD formationby block copolymer

KINETIC INVESTIGATION OF QD SYNTHESIS

The speed of QD production was studied in relation to the concentration of palladium precursors. Depending on the reaction mechanism, nanosynthesis usually consists of a few steps. The following equations describe the two phases involved in our work involving the use of Pd(II) chloride as a palladium precursor: the first is the reduction of Pd(II) to Pd(0), also known as nucleation; and the second is the autocatalytic development of palladium quantum dots.

$$\text{Pd(II)} + \text{Block copolymer} \xrightarrow{k_1} \text{Pd(0)} + \text{Oxidized block copolymer} \quad (1)$$

$$\text{Pd(II)} + \text{Block copolymer} + \text{Pd(0)} \xrightarrow{k_2} 2\text{Pd (0)} + \text{Oxidized block copolymer} \quad (2)$$

where k_1 is the nucleation rate constant and k_2 is the growth rate constant.

Watzky and Finke were the first to document this mechanism type (1997). Spectrophotometric analysis was used to examine the nucleation and growth kinetics of PdQDs under varying concentrations of metal ions. The following is the analytical solution of the differential equation (Eq. (1) and (2)) that describes the change of concentration of Pd(II) ions with time:

$$A_{Pd\,(II),t} = \frac{\frac{k_1}{k_2} + A_{Pd\,(II),0}}{1 + \frac{k_1}{k_2 . A_{Pd\,(II),0}} e^{\left(k_1 + k_2 . A_{Pd\,(II),0}\right).t}} \quad (3)$$

Thus, on one hand, we have the initial absorbance of palladium(II) ions (APd(II),0) and, on the other, the palladium absorbances (which change with time, t) that are proportional to the ion concentration according to Lambert-Beer's rule. Rates k_1 and k_2 are proportional to their corresponding observed rate values, $k_{1,obs}$ and $k_{2,obs}$, respectively.

Figure 7's inset indicates that when Pd(II) ions (0.033 - 0.233 mM) are added to the block copolymer, the absorbance values increase and the colour changes from brown to grey, as expected. These alterations in hue verify not only the nucleation and growth of QDs, but also the reduction of Pd ions.

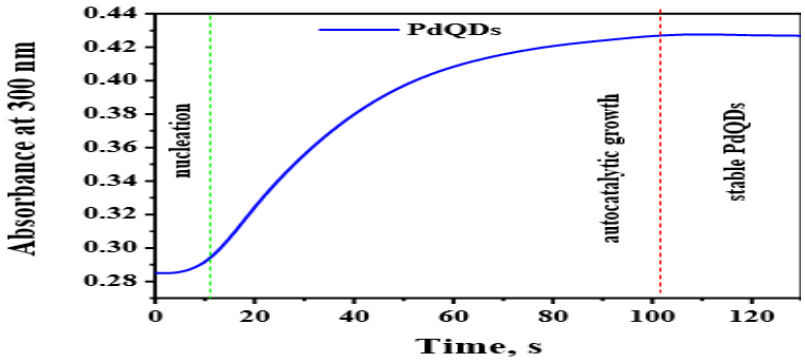

Figure 7: Typical sigmoidal kinetic curves of nucleation and growth process of PdQDs

Grey colloids show a more pronounced effect of a high palladium precursor concentration. This is a common occurrence when the concentration of the reagent is increased. Investigating the PdQDs' nucleation and growth rate provided more evidence supporting this assumption. The kinetic curves for the nucleation and growth rates of PdQDs as plasmons are displayed in figure 7. According to Wojnicki et al. (2016), the production of nanoparticles from precious metals is the only process that exhibits a sigmoidal kinetic curve. The delayed nucleation process and autocatalytic growth are both confirmed by this graph. As the concentration of Pd(II) increases, more nuclei will be generated at once, which is expected to speed up the process of nanoparticle creation. Equation 3 was used to derive the measured rate constants for the growth and nucleation processes. Remarkably, the predicted acceleration of nucleation as a result of a greater concentration of metal ions did not materialise. M. Wojnicki et al. (2016) already provided evidence for this observation in their report. It appears that the rate of nucleation is unaffected by the concentration of Pd(II) ions, as the k1,obs values are relatively constant (figure 8a). Therefore, it follows that the concentration range of nucleation is unaffected by both the diffusion process and the concentration of metal ions in the solution. Figure 8b shows that the palladium precursor had a pronounced influence on the $k_{2,obs}$ value. The growth rate constants were found to decrease when the concentration of Pd(II) ions increased. One way to mathematically describe this expansion is as:

$$k_{2,obs} = (2.893 \pm 0.144)\, C_{0,Pd(II)}^{(-1.110 \pm 0.055)} \quad (4)$$

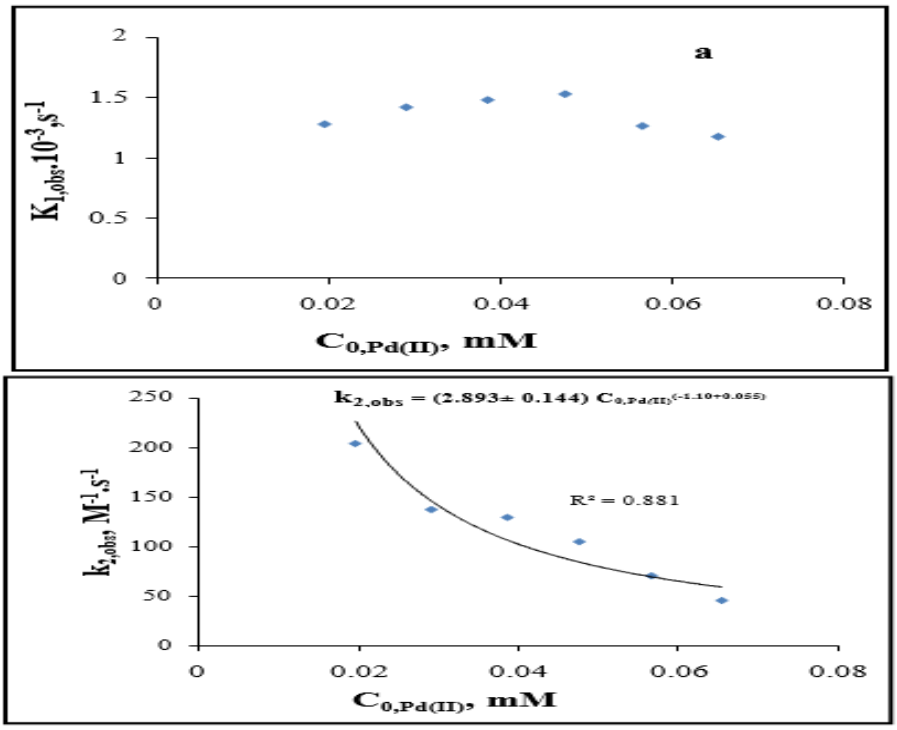

Figure 8: Observed rate constants for (a) nucleation (k_1)and (b) growth (k_2) process vs. initial concentration of Pd(II). Conditions: C_0, Pd(II) = 0.02—0.65 mM (a) k_1(b) k_2 of Pd NPs

USING PDQDS FOR THE CATALYTIC REDUCTION OF CR(VI) TO CR(III)

A 1 mL colloidal solution of PdQDs, produced as described earlier in the presence of 1.75 M acetic acid, was mixed with 1 mL of a 1 mM Cr(VI) solution to study the catalytic activity of PdQDs at room temperature. The decrease in the peak intensity related to Cr(VI) (λ_{max} =350 nm) was tracked by recording the absorbance both immediately after the solutions were added and after 24 hours. Another set of solutions was generated by adding varied concentrations of acetic acid to 1 mL of PdQD solution and 1 mL of 1 mM dichromate solution. This allowed us to further study the parameters impacting the reduction, specifically the acid content. We tracked the shift in the spectra at 350 nm. To study the impact of different ratios of QDs and dichromate on the reduction reaction, comparable sets were made and observed. By comparing the observed shifts in the absorption peaks to a standard calibration plot, we were able to ascertain the following Cr(VI) concentrations. We calculated the rate of change in Cr(VI) concentration as the percentage of change from the beginning value to the final value, with respect to time.

Effect of Concentration of Acetic Acid

By changing the quantity of acetic acid in a reaction mixture that already contained a set amount of catalyst—a 2 mL solution of colloidal PdQDs—and 1 mL of a 10 mM Cr(VI) solution, we were able to study the effect of acetic acid concentration. This was done to find out what the lowest acetic acid concentration needed to be for a very efficient reduction of Cr(VI). Using a constant concentration of PdQDs at room temperature, Figure 9a shows data acquired with varying amounts of acetic acid, whereas Figure 9b shows data obtained after 24 hours of reaction time. An improvement in reduction was noted as the concentration of acetic acid increased. When subjected to the experimental conditions, a reaction mixture containing 1.75 M acetic acid, 1 mL of 10 mM Cr(VI), and 2 mL of colloidal PdQDs was able to achieve full reduction after being in contact for 24 hours.

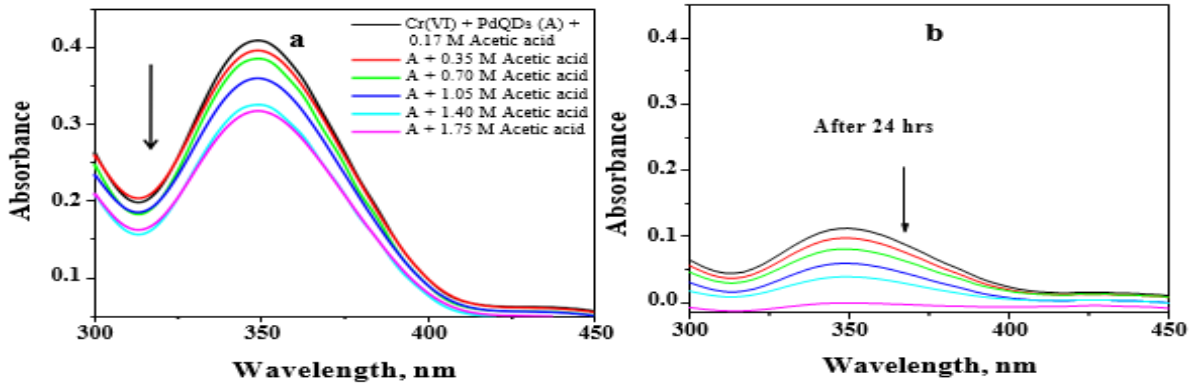

Figure 9: Analysis of Cr(VI) reduction by increasing conc. of acetic acid in the presenceof PdQDs (a) decrease in Cr(VI) absorbance at the characteristic absorption peak of 350 nm immediately (b) after 24h

5.9.3. Ratio of time to Cr(VI) reduction

The exponentially decreasing slopes in figure 10 show that the rates of reducing Cr(VI) to Cr(III) using acetic acid assisted PdQDs increase with increasing Cr(VI) concentration.

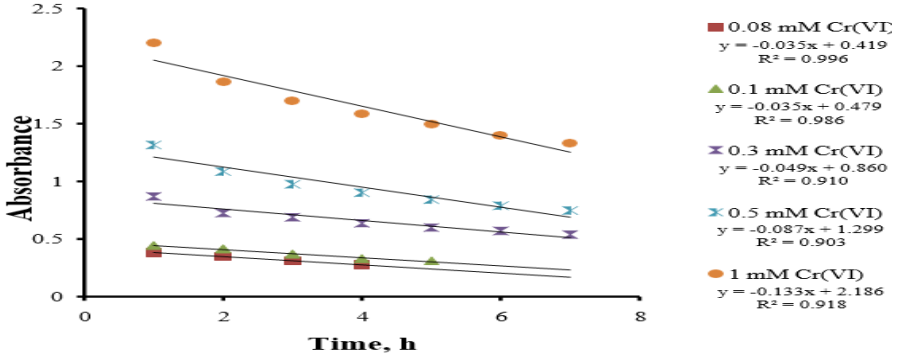

Figure 10: Order and rate of Cr(VI) reduction by PdQDs

By utilising the kinetic spectrophotometric methods described by Samaddar and Sen (2013), the rate constant and reaction order can be determined by plotting log V vs. log C, where V is the slope magnitude and C is the Cr(VI) concentration, as shown in equations 5 and 6. The rate of decrease of Cr(VI) can be described by taking the concentration of PdQD constant into account and writing it as

$$V = kC^n \quad (5)$$

the reaction order (n), the concentration of Cr(VI) (C), the rate constant (k), and the reaction rate (V) are all variables in this process. Here is an example of the logarithmic form of the equation:

$$\log V = \log k + n \log C \quad (6)$$

The order of the reaction can be seen in the slope (figure 11) of 1.75 (~2) and the rate constant (1.572 h^{-1}) of a plot of log V vs. log C. At any given moment throughout the catalytic reduction, this number would be useful for determining the concentration of an unknown Cr(VI). Equation (7) also shows the second order of the reaction.

$$Cr(VI) + CH_3COOH \xrightarrow{PdQDs} Cr(III) \quad (7)$$

whose rate equation is r = k[Cr(VI)][CH_3COOH]

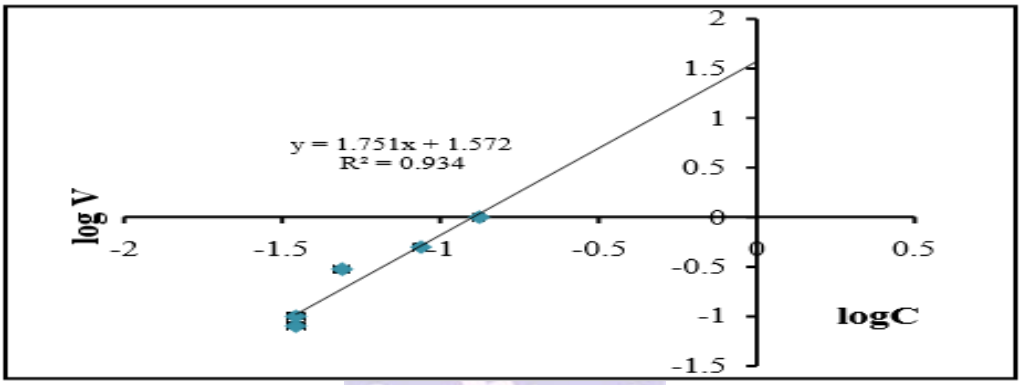

Figure 11: A plot of logV vs. logC to obtain the value of rate constant and order of the reaction.

CONCLUSIONS

A straightforward, one-pot process was developed for the synthesis of PdQDs. The given method has the potential to be disruptive and has several uses, but it is also easier to implement than other methods because it does not require specific equipment, can be done at room temperature, and does not use harsh chemicals. The creation of the PdQDs is confirmed by the results acquired from the characterisation techniques. A sigmoidal curve, seen in the absorption-based time scan spectra acquired during PdQD production, suggests that the nanoparticles grew autocatalytically. Due to their tiny size and monodispersed nature, the synthesised nanoparticles are excellent candidates for use in catalytic processes. The produced PdQDs were employed to reduce Cr(VI) to Cr(III) in the presence of acetic acid at room temperature. Utilising these material synthesised in this work, it is possible to achieve a complete reduction of the dangerous Cr(VI) to Cr(III). In this reduction reaction, the quantum dots likely worked as a catalyst because of their large surface area. The catalyst can be separated and reused after being γ irradiated onto the QDs, which leads to their aggregation and subsequent precipitation. It is possible to recycle the collected solid and utilise it to reduce Cr(VI) to Cr(III), but the efficiency will be lower than the first time. The greater size of the NPs generated during precipitation is mostly to blame for this. The rapid and quantitative response shown when γ irradiations are present is the most intriguing result. Using PdQDs as a catalyst in the development of effective Cr(VI) reduction systems is highly promising, despite the fact that Pd is an expensive reagent. By combining them with γ irradiations, even more progress can be achieved.

REFERENCES

1. Chawla M, Kumar R, Murielle PFS; J. Mol. Catal. A: Chem. 423 (2016) 126.
2. Elliott DW, Zhang W; Environ. Sci. Technol. 35 (2001) 4922.
3. Firouzabadi H, Iranpoor N, Ghaderi A; Org. Biomol. Chem. 9 (2011) 865.
4. Fu GT, Jiang X, Wu R, Wei SH, Sun DM, Tang YW, Lu TH, Chen Y; Appl. Mater. Inter. 6 (2014) 22790.
5. He YQ, Liu SP, Kong L, Liu ZF; Spectrochim. Acta Part A 61 (2005) 2861.
6. Islam RU, Witcomb MJ, Scurrell MS, Lingen EV, Otterloc WV, Mallick K; Catal. Sci. Technol. 1 (2011) 308.
7. Jiang L, Wang W, Wu D, Zhan J, Wang Q, Wu Z, Jin R; Mater. Chem. Phys. 104 (2007) 230.
8. Kannan R, Kim AR, Dong JSK, Yoo JS; Int. J. Hydrogen Energy 41 (2016) 18033.
9. Kaune G, Ruderer MA, Metwalli E, Wang W, Couet S, Schlage K, Rohlsberger R, SV Roth, Buschbaum PM; ACS Appl. Mater. Interfaces 1 (2009) 353.
10. Kora AJ, Rastogi L; Arabian J. Chem. 2015 http://dx. doi. org /10. 1016 /j.arabjc. 2015. 06.024.
11. Oberhauser W, Bartoli M, Petrucci G, Bandelli D, Frediani M, Capozzoli L, Cepek C, Bhardwaj S, Rosib L; J. Mol. Catal. A: Chem. 410 (2015) 26.
12. Omole MA, K'Owino IO, Sadik OA; Appl. Catal. B 76 (2007) 158 Raluy E, Favier I, Vinasco AML, Pradel C, Martin E, Madec D, Teuma E, Gomez M; Phys. Chem. Chem. Phys. 13 (2011) 1357.